DRAFT VERSION JANUARY 25, 2010
Preprint typeset using LaTeX style emulateapj v. 11/26/03

WHERE DO WET, DRY, AND MIXED GALAXY MERGERS OCCUR? A STUDY OF THE ENVIRONMENTS OF CLOSE GALAXY PAIRS IN THE DEEP2 GALAXY REDSHIFT SURVEY

LIHWAI LIN [1], MICHAEL C. COOPER [2,3], HUNG-YU JIAN [4], DAVID C. KOO [5], DAVID R. PATTON [6], RENBIN YAN [7], CHRISTOPHER N. A. WILLMER [2], ALISON L. COIL [8], TZIHONG CHIUEH [4], DARREN J. CROTON [9], BRIAN F. GERKE [10], JENNIFER LOTZ [11,12], PURAGRA GUHATHAKURTA [5], AND JEFFREY A. NEWMAN [13]

Draft version January 25, 2010

ABSTRACT

We study the environment of wet, dry, and mixed galaxy mergers at $0.75 < z < 1.2$ using close pairs in the DEEP2 Galaxy Redshift Survey, aiming to establish a clear picture of how the cosmic evolution of various merger types relate to the observed large-scale extra-galactic environment and its role in the growth of red-sequence galaxies. We find that the typical environment of mixed and dry mergers is denser than that of wet mergers, mostly due to the color-density relation. While the galaxy companion rate (N_c) is observed to increase with overdensity, using N-body simulations we find that the fraction of pairs that will eventually merge decreases with the local density, predominantly because interlopers are more common in dense environments. After taking into account the merger probability of pairs as a function of local density, we find only marginal environment dependence of the fractional merger rate for wet mergers over the redshift range we have probed. On the other hand, the fractional dry merger rate increases rapidly with local density due to the increased population of red galaxies in dense environments. In other words, while wet mergers transform galaxies from the blue cloud into the red sequence at a similar fractional rate across different environments (assuming that the success rate of wet mergers to yield red galaxies does not depend on environment), the dry and mixed mergers are most effective in overdense regions. We also find that the environment distribution of K+A galaxies is similar to that of wet mergers alone and of wet+mixed mergers, suggesting a possible connection between K+A galaxies and wet and/or wet+mixed mergers. Based on our results, we therefore expect that the properties, including structures and masses, of red-sequence galaxies should be different between those in underdense regions and in overdense regions since the dry mergers are significantly more important in dense environments. We conclude that, as early as $z \sim 1$, high-density regions are the preferred environment in which dry mergers occur, and that present-day red-sequence galaxies in overdense environments have, on average, undergone 1.2 ± 0.3 dry mergers since this time, accounting for $(38\pm10)\%$ of their mass accretion in the last 8 billion years. Our findings suggest that dry mergers are crucial in the mass-assembly of massive red galaxies in dense environments, such as Brightest Cluster Galaxies (BCGs) in galaxy groups and clusters.

Subject headings: galaxies:interactions - galaxies:evolution - large-scale structure of universe

1. INTRODUCTION

Within the framework of hierarchical structure formation, dark-matter halos grow through successive mergers with other halos and through accretion of the surrounding mass (Blumenthal et al. 1984; Davis et al. 1985; Stewart et al. 2009). Whether this bottom-up scenario also holds for galaxies which reside in dark matter halos remains a challenging question in the theories of galaxy formation and evolution. The keys to pin down the importance of mergers in the assembly history of galaxies are the study of galaxy merger rates as a function of cosmic time (Carlberg et al. 2000; Patton et al. 2002; Conselice et al. 2003; Lin et al. 2004, 2008; Lotz et al. 2008a; de Ravel et al. 2009; Bluck et al. 2009) and to understand the level of triggered star formation during galaxy interactions (Lambas et al. 2003; Nikolic et al. 2004; Woods et al. 2006; Lin et al. 2007; Barton et al. 2007; Ellison et al. 2008).

In addition to assembling galaxy masses, galaxy mergers have also been suggested to be responsible for the change of galaxy properties (Hopkins et al. 2006). Galaxy populations have been shown to evolve differently since redshift 1.5: while the characteristic number densities of blue galaxies remain fairly constant, the number and stellar mass densities of red galaxies have at least doubled over this period (Bell et al. 2004; Willmer et al. 2006; Faber et al. 2007). The growth rate of the red galaxies is much faster than the predictions from purely passive evolution, suggesting that additional physical mechanisms are required to truncate the star formation in some of the blue galaxies and turn them into the red-sequence (Bell et al. 2007). More recently, there have been studies examining the connection between galaxy mergers and the

[1] Institute of Astronomy & Astrophysics, Academia Sinica, Taipei 106, Taiwan; Email: lihwailin@asiaa.sinica.edu.tw
[2] Steward Observatory, University of Arizona, 933 N. Cherry Avenue, Tucson, AZ 85721 USA
[3] Spitzer Fellow
[4] Department of Physics, National Taiwan University, Taipei, Taiwan
[5] UCO/Lick Observatory, Department of Astronomy and Astrophysics, University of California, Santa Cruz, CA 95064
[6] Department of Physics and Astronomy, Trent University, 1600 West Bank Drive, Peterborough, ON K9J 7B8 Canada
[7] Department of Astronomy and Astrophysics, University of Toronto, 50 St. George Street, Toronto, ON M5S 3H4, Canada
[8] Department of Physics and Center for Astrophysics and Space Sciences, University of California, San Diego, 9500 Gilman Dr., La Jolla, CA 92093
[9] Centre for Astrophysics & Supercomputing, Swinburne University of Technology, P.O. Box 218, Hawthorn, VIC 3122, Australia
[10] Kavli Institute for Particle Astrophysics and Cosmology, Stanford Linear Accelerator Center, 2575 Sand Hill Rd., M/S 29, Menlo Park, CA 94025, USA
[11] National Optical Astronomy Observatory, 950 N. Cherry Ave., Tucson, AZ 85719
[12] Leo Goldberg Fellow
[13] Physics and Astronomy Dept., University of Pittsburgh, Pittsburgh, PA, 15620

establishment of red-sequence galaxies (van Dokkum 2005; Bell et al. 2006; Lin et al. 2008; Skelton et al. 2009). Using close pairs found in the DEEP2 Survey, Lin et al. (2008) found that the present red galaxies might have experienced on average 0.7, 0.2, and 0.4 wet, dry, and mixed mergers respectively since $z \sim 1$, suggesting a key role of galaxy mergers in the evolution history of red galaxies. In addition, the relative role of different types of mergers also evolve with redshift, indicating that the effect of quenching star formation and mass build-up through mergers also evolve with time. Meanwhile, it becomes increasingly clear that dense regions such as galaxy groups and clusters might be the places where the transformation of blue galaxies into red galaxies occurs most effectively. If galaxy mergers are the dominant quenching mechanism, one should also expect a clear environment dependence of galaxy merger rates. However, there have been very few attempts to probe the connection between mergers and environment observationally (McIntosh et al. 2008; Darg et al. 2009).

Another way to probe the connection between mergers and the formation of red galaxies is to compare the environment distribution of mergers to the poststarburst galaxies, the so-called 'K+A' or 'E+A' galaxies (Dressler & Gunn 1983). Such galaxies are identified through their strong Balmer absorption and little Hα or [OII] emissions, indicating that they had recent star formation with the last ~ 1 Gyr or so, but no on-going star formation. These K+A galaxies are suggested to be the transition phase between star forming galaxies and the dead red-sequence galaxies, and hence they could be the direct progenitors of early-type red galaxies. There have been many studies looking at the environment of poststarburst galaxies (Goto 2005; Hogg et al. 2006; Yan et al. 2009; Poggianti et al. 2008), with the aim of identifying the process that truncates the star formation activity (mergers, ram-pressure stripping, AGN feedback, etc.). By comparing the environment distribution of K+A galaxies in the literature to that of galaxy mergers, we can gain insight on the importance of galaxy mergers in the formation of K+A galaxies and hence the built-up of red-sequence galaxies.

Since galaxy interactions require more than one galaxy by definition, it is expected that galaxy mergers tend to reside in dense regions. Galaxy groups are thought to be preferred places for galaxy mergers because of their lower velocity dispersions as opposed to the galaxy clusters. By studying four X-ray luminous groups at intermediate redshifts ($z \sim 0.4$), Tran et al. (2008) suggested that dry mergers are an important process to build up massive galaxies in the cores of galaxy groups/clusters; McIntosh et al. (2008), using group and cluster samples in SDSS also found that the frequency of mergers between luminous red galaxies (LRGs) is significantly higher in groups and clusters compared to overall population of LRGs. While most of previous studies examining the environment of mergers focused on the dry mergers in dense environments, to date no quantitative measurement of wet, dry, and mixed merger rates as a function of environment has been obtained. This paper aims to address the issue of where galaxies build up their masses and where the transformation of galaxies happens by exploring the environment of various types of interacting galaxies. There are two methods that have been used in DEEP2 to classify environments: one is to use the projected n^{th}-nearest neighbor surface density Σ_n (Cooper et al. 2006), which gives the estimates of local density of individual galaxies; the other is to classify the galaxy environments into "field" and "groups/clusters" (Gerke et al. 2005). In this work, we adopted the former approach as a primary environment measurement to investigate (1) which environment hosts most wet/dry/mixed mergers and (2) the pair fraction and the fractional merger rate as a function of environment at $0.75 < z < 1.2$, using the blue-blue, red-red, and blue-red pairs selected from the DEEP2 sample (Lin et al. 2008). It is worth noting that there are potential caveats in our analysis using galaxy colors to classify wet/dry/mixed mergers. At $z \sim 1$, it is found that about 20% of red galaxies appear to be either edge-on disks or dusty galaxies and hence are likely to be gas-rich (Weiner et al. 2005) whereas there also exist blue spheroidals that could be gas-poor, although these are relatively rare objects (Cassata et al. 2007). As noted in Lin et al. (2008) that both cases of contamination make up only a minority of the red sequence and blue clouds respectively, classifying different types of mergers based on their colors should be a fair approximation.

Major uncertainties in converting the pair fraction into the merger fraction and merger rates come from the handling of the fraction of pairs that will merge C_{mg} and merger time-scale T_{mg} (Kitzbichler & White 2008; Lotz et al. 2008b). The most common way of assessing merger time-scale is computed as the "dynamical friction time" (Binney & Tremaine 1987; Wetzel et al. 2009) or is estimated from the N-body/hydrodynamic simulations of galaxy mergers (Conselice 2006; Jiang et al. 2008; Lotz et al. 2008b). On the other hand, the fraction of pairs selected with projected separation with/without the line-of-sight velocities that are physically-associated pairs and will merge within a short time is often obtained by correcting for chance projection (Patton & Atfield 2008; Bundy et al. 2009). Both T_{mg} and C_{mg} are usually assumed to be a constant at a given redshift and mass bin, independent of the environment. However, such approaches may not be adequate when comparing the merger rate across different environments because close pairs in dense environments are not simply isolated two-body systems, but are also influenced by nearby galaxies, surrounding material, and the gravitational potential from the group/cluster host halos. In order to make a fair comparison of merger frequencies across various environments, we adopt an improved estimate of T_{mg} and C_{mg} as a function of environment obtained from cosmological simulations when converting the pair fraction into the fractional merger rate.

The paper is organized as follows. In §2, we describe our sample selection and the approach of measuring environment. In §3, we present our results on the pair fractions for blue and red galaxies, the computation of both T_{mg} and C_{mg}, as well as the derived fractional merger rates for different merger categories. A discussion is given in §4, followed by our conclusions in §5. Throughout this paper we adopt the following cosmology: $H_0 = 100h$ km s^{-1} Mpc^{-1}, $\Omega_m = 0.3$ and $\Omega_\Lambda = 0.7$. The Hubble constant $h = 0.7$ is adopted when calculating rest-frame magnitudes. Unless indicated otherwise, magnitudes are given in the AB system.

2. DATA, SAMPLE SELECTIONS, AND METHODS

2.1. *The DEEP2 Redshift Survey*

The DEEP2 Redshift Survey (DEEP2 for short) has measured redshifts for $\sim 50,000$ galaxies at $z \sim 1$ (Davis et al. 2003, 2007) using the DEIMOS spectrograph (Faber et al. 2003) on the 10-m Keck II telescope. The survey covers four fields with Field 1 (EGS: Extended Groth Strip) being a strip of 0.25×2 square degrees and Fields 2, 3 and 4 each being 0.5×2 square degrees. The photometry is based on *BRI* images taken with the 12K$\times$8K camera on the Canada-France-

Hawaii Telescope (Coil et al. 2004). Galaxies are selected for spectroscopy using a limit of $R_{AB} = 24.1$ mag. Except in Field 1, a two-color cut was also applied to exclude galaxies with redshifts $z < 0.75$. A 1200 line/mm grating (R $\sim$ 5000) is used with a spectral range of $6400-9000$ Å, where the [OII] 3727 Å doublet would be visible at $z \sim 0.7-1.4$. The data used here contains $\sim 20,000$ galaxies with reliable redshift measurements from Fields 1, 3 and 4. The rest-frame B-band magnitudes (M_B) and $U-B$ colors for DEEP2 galaxies at $0.75 < z < 0.9$ are derived in a similar way as Willmer et al. (2006). For galaxies with $0.9 < z < 1.2$, the rest-frame $U-B$ color is computed using the observed $R-z_{\rm mega}$ color whenever it is available, where $z_{\rm mega}$ is the z-band magnitude obtained from CFHT/Megacam observations for DEEP2 Fields in 2004 and 2005 (Lin, L. et al., in preparation).

2.2. *Close Pair Sample in DEEP2*

The DEEP2 close pairs used in this work are identical to those described in Lin et al. (2008). We begin with a sample of galaxies covering $-21 < M_B^e < -19$ (AB mag), where M_B^e is the evolution-corrected absolute magnitude, defined as M_B+ Qz. The value of Q is chosen to be 1.3 in order to select galaxies with the same range relative to the L^* of the evolving luminosity function (Faber et al. 2007). Kinematic close pairs are then identified such that their projected separations (r_p) satisfy 10 h^{-1}kpc $\leq r_p \leq r_{max}$ (physical length) and rest-frame relative velocities ($|\Delta v|$) are less than 500 km s^{-1} (Patton et al. 2000; Lin et al. 2004). In this work, we identify the pairs using r_{max} = 50 h^{-1}kpc in order to have sufficient sample when dividing pairs into several different environment bins.

Galaxies are further divided into the blue cloud and red sequence using the rest-frame magnitude dependent cut for DEEP2 (in AB magnitudes):

$$U-B = -0.032(M_B + 21.62) + 1.035. \quad (1)$$

Blue-blue pairs, red-red pairs, and blue-red pairs are classified according to the rest-frame $U-B$ color combination of the galaxies comprising the pair, representing the candidates of 'wet', 'dry', and 'mixed' mergers (Lin et al. 2008). In total, we have 101 blue-blue pairs, 26 red-red pairs, and 52 blue-red pairs over the redshift range $0.75 < z < 1.2$.

2.3. *Local Environment Indicator*

For each galaxy in the DEEP2 redshift sample, the local density environment is measured using the projected third-nearest-neighbor surface density (Σ_3). The detailed procedure is described in Cooper et al. (2005, 2006). Here we briefly summarize the steps of computing the overdensity δ_3 used in this work. Σ_3 is first calculated as $\Sigma_3 = 3/(\pi D_{p,3}^2)$, where $D_{p,3}^2$ corresponds to the projected distance of the third-nearest neighbor that is within the line-of-sight velocity interval of $\pm$1000 km s^{-1} . For each galaxy, we then derive the overdensity δ_3 as the local-sky completeness-corrected density Σ_3/w_p, denoted as $\Sigma_3{}'$, divided by the median density $\Sigma_3{}'(z)$ at that redshift computed in bins of $\triangle z = 0.04$:

$$1+\delta_3 = \Sigma_3'/\mathrm{median}(\Sigma_3'(z)), \quad (2)$$

where w_p is the local-sky completeness. $(1+\delta_3)$ is thus a measure of the overdensity relative to the median density, which takes into account the variation in the redshift dependence of the sampling rate. As discussed in Cooper et al. (2005), δ_3 is shown to be a robust environment measure for the DEEP2 sample.

2.4. *Galaxy Group Catalogs*

Although the overdensity δ_3 is a good representation of local environment, it does not carry specific information regarding what kind of physical environment like field, groups, and clusters it corresponds to. A complementary way to classify the environment is to cross reference the galaxy sample to the group/cluster catalogs. However, performing the group/cluster finding is not always possible, depending on the availability of redshifts, sampling rate, and other wavelength data (e.g. X-ray). DEEP2 targeted $\sim$ 65% of all of the galaxies down to R=24.1, and $\sim$ 70% of these galaxies yield successful redshifts. Hence the overall redshift sampling rate of DEEP2 is about 50%, which allows identifying potential group candidates. The group catalog used in this paper is based on the version generated by Gerke et al. (2007), who applied the Voronoi-Delaunay Method (VDM) group finder (Marinoni et al. 2002) on the DEEP2 redshift sample. For detailed discussion on the DEEP2 group catalog, see Gerke et al. (2005, 2007). It was shown that this group catalog is most sensitive to groups with modest virial masses in the range $5\times10^{12} < M_{vir} < 5\times10^{13} M$ ($200 < \sigma_v < 400$ km s^{-1}) (Coil et al. 2006). In §3.2, we present the distributions of various types of pairs against group properties. However, due to the incompletenss of group member identifications in the DEEP2 sample, we therefore focus our final discussion on the results obtained using the local density measurements.

2.5. *The selection function and the spectroscopic weight*

As mentioned in §2.4, the overall redshift sampling rate of DEEP2 is about 50%, which has an impact on measuring the true pair fraction and hence the merger rate. In order to recover the intrinsic number of pairs, one must consider the completeness corrections accounting for the spectroscopic selection effects. Detailed calculations and results of the DEEP2 selection functions were presented in our previous work (Lin et al. 2008); here we summarize main steps of these calculations. To measure the spectroscopic weight w for each galaxy in the DEEP2 survey, we compared the sample with successful redshifts to all objects in the photometric catalog that satisfy the survey's limiting magnitude and any photometric redshift cut. We parameterize the selection function to be (Lin et al. 2008; Yee et al. 1996; Patton et al. 2002):

$$S = S_m\,\overline{S_c}\,\overline{S_{SB}}\,\overline{S_{xy}} = S_m(R)\frac{S_c(B-R,R-I,R)}{S_m(R)}\frac{S_{SB}(\mu_R,R)}{S_m(R)}\frac{S_{xy}}{S_m(R)}, \quad (3)$$

where S_m is the magnitude selection function, S_c is the apparent color selection function, S_{SB} is the surface brightness selection function and S_{xy} represents the geometric (local density) selection function. $\overline{S_c}$, $\overline{S_{SB}}$, and $\overline{S_{xy}}$ are all normalized to the magnitude selection function, S_m. The spectroscopic weight w for each galaxy is thus $1/S$, which is derived from its apparent R mag, $B-R$ and $R-I$ colors, R band surface brightness, and local galaxy density.

The magnitude selection function $S_m(R)$ for each galaxy is computed as the ratio between the number of galaxies with good redshift qualities to the total number of galaxies in the target catalog in both cases, considering a magnitude bin of $\pm$0.25 mag centered on the magnitude and colors of the galaxy. The color selection function $S_c(B-R,R-I,R)$ is computed by counting galaxies within $\pm$ 0.25 R magnitude over a $B-R$ and $R-I$ color range of $\pm$ 0.25 mag. Similarly, the surface brightness selection function is defined within $\pm$0.25 mag in μ_R and $\pm$ 0.25 mag in R. The geometric selection

function $S_{xy}(xy,R)$ is similar to the magnitude selection function but computed on a spatially-defined (i.e., localized) scale. We take the ratio between the number of galaxies with good quality redshifts and the total number in the targeted catalog in an area of radius 120" within a $\pm$ 0.25 R-magnitude range.

Besides the selection function for each individual galaxy, we also investigate the selection dependence on pair separation. We measure the angular separation of all pairs in the redshift catalog (z-z pairs) and in the target catalog (p-p pairs) respectively and then count the number of pairs (N_{zz} and N_{pp}) within each angular separation bin. While counting the pairs in the redshift catalog, each component of the pair counts is weighted by the geometric selection function $S_{xy}(xy)$ to exclude any effect due to the variance in the local sampling rate. The angular selection function S_θ is computed as the ratio between the weighted N_{zz} and N_{pp}. The angular weight, w_θ, for each galaxy is hence $1/S_\theta$.

3. RESULTS

3.1. *Environment Distribution of Blue-Blue/Red-Red/Mixed Pairs*

Fig. 1(a) shows the projected positions of wet, dry, and mixed pairs found in one of the DEEP2 fields (Field 4), overlaid with contours tracing the mean density along the line-of-sight. Visually it reveals that blue-blue pairs appear in all kinds of environments, from low to high density regions. On the other hand, red-red pairs and blue-red pairs tend to lie in denser environments. Quantitative comparisons between the local environment of the three types of pairs, after correcting for the spectroscopic incompleteness, are shown in Fig. 1(b). We first note that all blue-blue, red-red, and blue-red pairs have median local density greater than the average environment ($\log_{10}(1+\delta_3)\ \sim 0$). This is expected: paired galaxies, by definition, have a close companion nearby and thus their separation from the 3^{rd}-nearest neighbor will be smaller (and hence denser) on average by construction. The most interesting result of Fig. 1(b) lies in the difference in the density distribution among blue-blue, red-red, and blue-red pairs. While blue-blue pairs favor median-density environments, red-red and blue-red pairs are preferentially located in overdense regions.

To better understand whether such density distribution of pairs is related to the color-density relation, i.e., the change of the fraction of red galaxies across different local densities (Hogg et al. 2004; Cooper et al. 2006; Cucciati et al. 2006), we perform the following analysis: for a given local density, we compute the red-galaxy fraction corrected by the spectroscopic incompleteness, and then derive the predicted relative fraction among wet, dry, and mixed pairs assuming that the red and blue galaxies are randomly distributed. As illustrated in Fig. 1(c), the increased fractions of dry and mixed pairs with respect to the local density follow a similar trend as expected from the color-density relation. However, we find an excess of dry and mixed pairs toward overdense regions at a $\sim$ 2-σ level compared to the above expectation, indicating that the red and blue galaxies are not uniformly distributed and that there exists a clustering effect at very small scales in those overdense environments.

.

The difference in the density distribution of wet/dry/mixed mergers suggests that the physical environment where various types of mergers occur is essentially different. To interpret our results, we also investigate how different mergers are populated as a function of the velocity dispersion and the number of members of galaxy groups for a subset of DEEP2 samples that have group identifications as presented in Gerke et al. (2007). The two upper panels of Fig. 2 plot the overdensity against velocity dispersion (left) and the number of group members (right) for paired galaxies. As expected, there is a clear trend that the local density of galaxies belonging to groups with greater velocity dispersion or group members is on average larger. This illustrates that the local environment measure δ_3 used in this work in general correlates well with physical environments (field, groups, clusters). As shown in the two bottom panels of Fig. 2, the fraction of red-red and blue-red pairs in groups with greater velocity dispersion or more group members is significantly higher than that of blue-blue pairs. More specifically, the majority of blue-blue pairs are found in field-like environments while red-red and blue-red pairs tend to be found in group and/or cluster-like environments.

It is worth pointing out that there are $\sim$ 11% of the pair sample whose two members do not belong to the same group. This can happen when a single group is split into two or more smaller groups by the group finder, or a group is not properly identified owing to the incompleteness of the spectroscopic sample. As a result, there are some pairs that are identified as 'field galaxy' based on the group finder. These are the paired galaxies assigned to have one group member as shown in the lower-right panel of Fig. 2. Such an effect makes the group results rather hard to interpret compared to the local density results, which are relatively insensitive to the spectroscopic incompleteness. We therefore focus on the discussion of the environment effects based on the results using the local density in the rest part of this paper.

3.2. *The Environment dependence of the Pair Fraction*

The above analysis on the environment distributions of wet/dry/mixed merging galaxy pairs provides insight into which environments play host to most galaxy mergers. However, this is different from asking in which environments galaxy mergers are more likely to occur. In this section, we investigate the latter issue by studying the relative frequency of galaxy interactions across different environments, i.e., to count the paired galaxies relative to the parent sample as a function of environment. We note that the pair fraction does not necessarily correspond to the merger fraction because not every kinematic pair defined observationally will eventually merge into one system. Such phenomenon is in particular more frequent in dense environments due to chance projection as well as many-body interactions. We will address this issue in §3.3 and §3.4.

The method we adopt to compute the pair fraction, N_c , is the same as described in our previous work (see §3.1 of Lin et al. 2008), except that we further bin the sample by the local densities. The pair fraction N_c is defined as the average number of companions per galaxy:

$$N_c = \frac{\sum_{i=1}^{N_{tot}} \sum_j w_j w(\theta)_{ij}}{N_{tot}}, \tag{4}$$

where N_{tot} is the total number of galaxies within the chosen absolute magnitude range, w_j is the spectroscopic weight for the jth companion belonging to the ith galaxy, and $w(\theta)_{ij}$ is the angular selection weight for each pair as described in §2.5. The averaged value of the overall spectroscopic weight w of our paired galaxies is about 2.1 and that of the angular selection weight is about 1.2 in the redshift range of $0.75 < z < 1.2$.

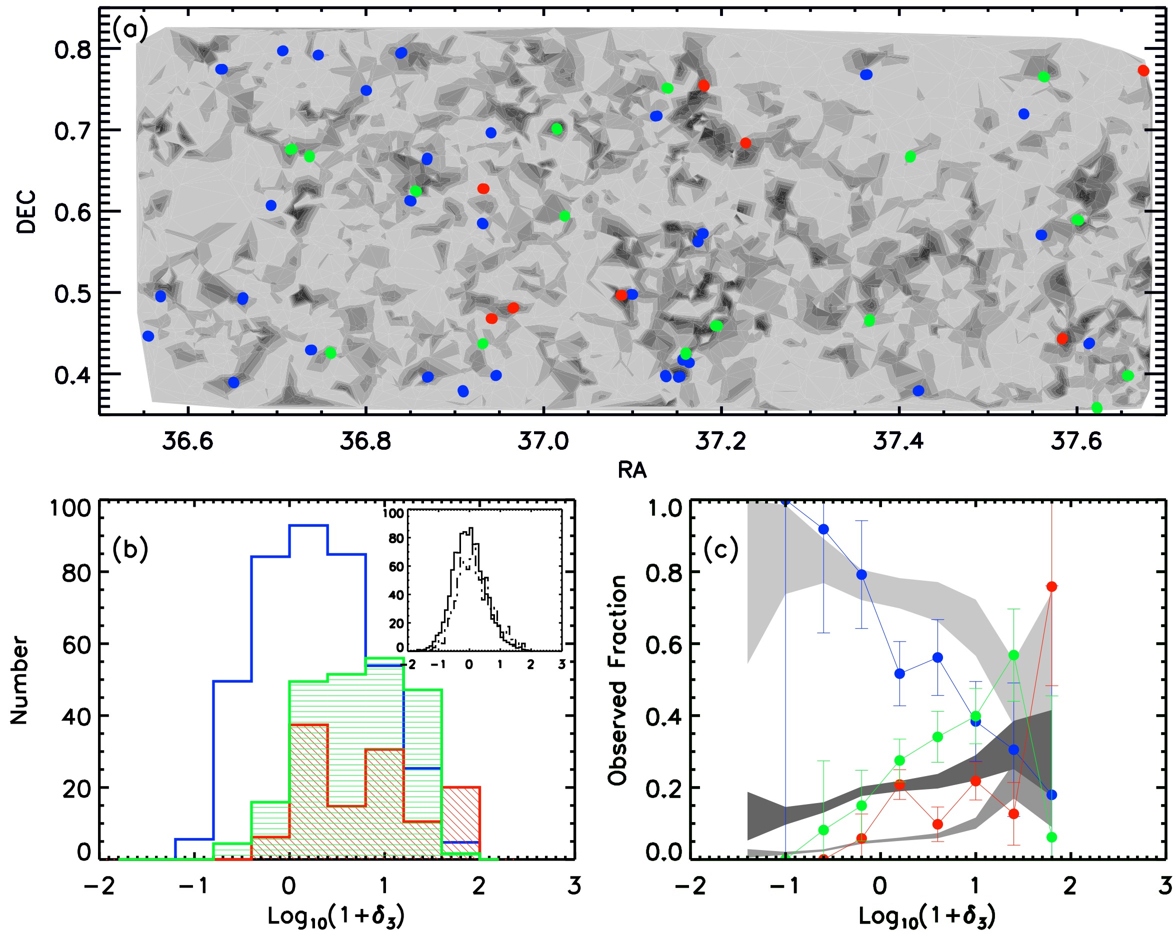

FIG. 1.— (a) The locations of blue-blue (blue dots), red-red (red dots), and blue-red (green dots) pairs in the DEEP2 Field 4, representing candidates of wet, dry, and mixed mergers respectively in part of the DEEP2 spectroscopic sample at $0.75 < z < 1.2$. The grey contours represent the overdensity $\log_{10}(1+\delta_3)$ with 6 levels: < 0, 0 - 0.3, 0.3 - 0.6, 0.6 - 0.9, 0.9 - 1.2, and > 1.2 (from light to dark). (b) The distribution of local density, $(1+\delta_3)$, for paired galaxies weighted by their spectroscopic incompleteness and angular selection functions. The paired sample is again divided into b-b (blue histogram), r-r (red histogram), and b-r (green histogram) pairs. The $(1+\delta_3)$ distributions of the blue/red galaxies of the full sample are also shown as black solid/dash-dotted lines for comparison (the numbers of blue and red galaxies have been reduced by a factor of 12 and 4 respectively). It is clearly seen that mixed and dry mergers occur in denser environments than wet mergers do. (c) The relative fraction of b-b (blue symbols), r-r (red symbols), and b-r (green symbols) pairs as a function of $(1+\delta_3)$. The error bars represent Poisson errors. The 1-σ predictions based on the observed color-density relation are shown as grey areas for comparison (light to dark: wet, dry, and mixed pairs). Our comparison shows that the observed relative fraction of the three types of pairs can be explained by the change of red-galaxy fraction across different local densities. In overdense regions, however, there exists a 2-σ difference between the observed pair fractions and the predictions following the color-density relation, which indicates that the clustering of blue and red galaxies at small scales may be different in those environments.

A correction factor of 2.4 in addition to the usual spectroscopic and angular separation corrections is also applied for each red companion at $z > 1$ to account for the missing faint red galaxies in the high-redshift DEEP2 sample (Lin et al. 2008). Four types of pair fraction are measured here: a) N_c from all pairs regardless of colors; b) the average number of blue companions per blue galaxy N_c^b ; c) the average number of red companions per red galaxy N_c^r ; d) the average number of companions of galaxies with opposite color to that of the primary galaxies N_c^m . Note that b) and c) are equivalent to the pair fraction within the blue cloud and red sequence, respectively. Here we divide the environment into three regimes: underdense environment, intermediate environment, and overdense environment. Naively one would think that the pair fraction should increase with the local density. In fact, this is not necessarily true for the blue pair fraction (N_c^b), red pair fraction (N_c^r), or mixed pair fraction (N_c^m) individually. One must keep in mind that the overdensity is computed using all galaxies of all colors and not segregated by galaxy colors. Therefore how the N_c^b , N_c^r , and N_c^m vary against environment depends on the relative red and blue fraction at a given environment, as discussed in §3.1

Fig. 3 displays the pair fraction as a function of overdensity $(1+\delta_3)$ in log space for two redshift bins $0.75 < z < 1.0$ and $1.0 < z < 1.2$. The rapid rise of N_c with increasing density is similar for all four types of pairs for the two redshift bins considered. However, the relative companion rate among wet/dry/mixed pairs changes across different environments. In underdense regions, the blue companion rate for blue galaxies (blue points) is in general higher than the red companion rate for red galaxies (red points). On the other hand, the opposite holds in overdense environments. This suggests that while the overall companion rate is enhanced in dense environments, the level of enhancement depends on the types of galaxies. In order to visualize the enhancement of the companion rate as a function of environment, the global values of N_c at a given redshift obtained by Lin et al. (2008) are also shown as horizontal arrows in each panel of Fig. 3. Quan-

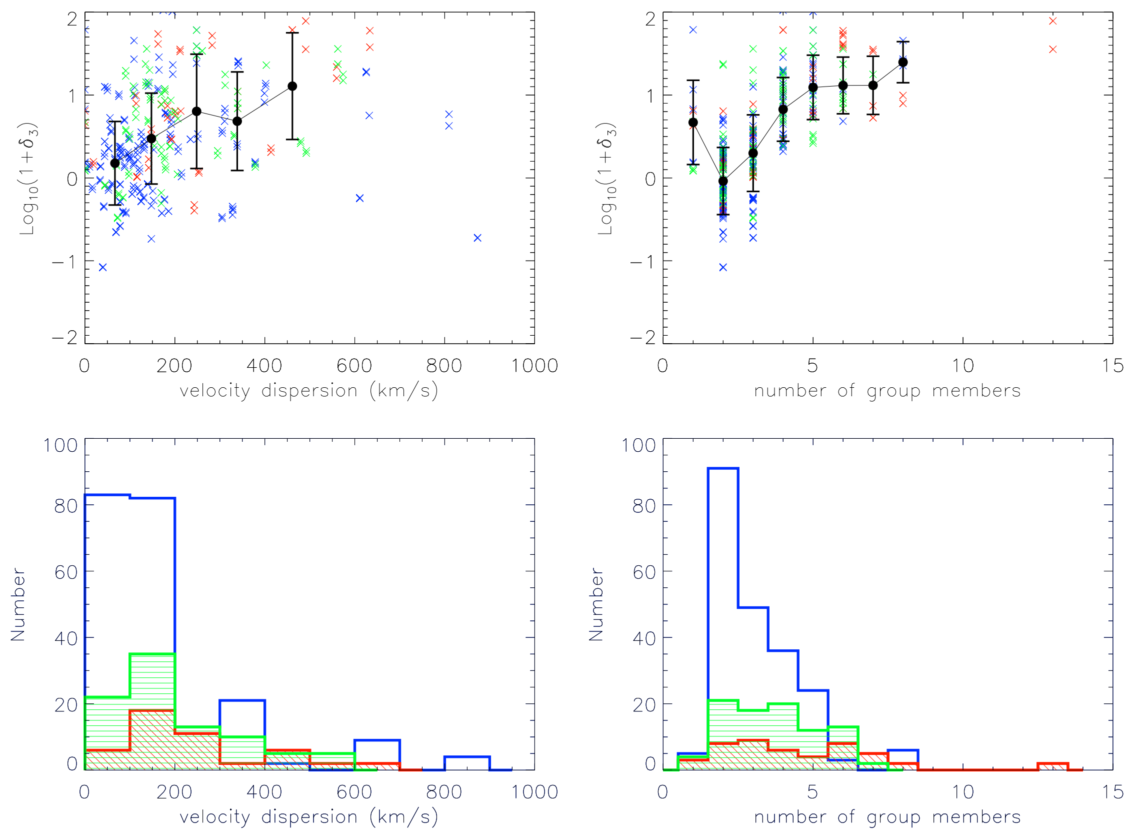

FIG. 2.— The two upper panels plot the overdensity against velocity dispersion (left) and the number of group members (right) for paired galaxies. The black symbols and associated error bars indicate the median value with the root-mean-squared of the scatter in each bin. The two lower panels display the histograms of velocity dispersion of groups and the number of group members for groups that host paired galaxies. Blue, green, and red colors denote for blue-blue, red-red, and blue-red pairs respectively.

titatively speaking, the companion rate is about 1.3-5 times greater in high-density regions compared to the global rate, depending on the type of pair.

3.3. *Estimates of C_{mg} and T_{mg} as a Function of the Local Environment*

As mentioned in §3.2, the pair fraction is not equal to the galaxy merger fraction unless all pairs are merging systems. It is possible that the pair sample is subject to contamination from interlopers owing to the difficulty of disentangling the Hubble expansion and the galaxy peculiar velocity. In order to take into account any possible environment effect on the merger time-scale (T_{mg}) and the fraction of merger in pairs (C_{mg}), we construct a mock galaxy catalog based on the dark matter halos and subhalos taken from a cosmological N-body simulation, and trace merger histories of halo-halo pairs to examine the dependence of C_{mg} and T_{mg} on the local density. A full description will be presented in a forthcoming paper (Jian, H.-Y. et al., in preparation). Here we briefly describe the techniques that are used to study this problem and present the most relevant results. We make use of the cosmological N-body simulations and the dark matter halos as presented in Jian et al. (2008). The simulation used here has been evolved in the concordance flat ΛCDM model: $\Omega_m = 0.3$, $\Omega_\Lambda = 0.7$, and $\Omega_b = 0.05$. It contains 512^3 pure dark matter particles in a 100 h^{-1} Mpc box on a side. The resulting mass of a dark matter particle is $m_{dm} = 6.188 \times 10^8 h^{-1} M_\odot$. The distinct halos and substructures (subhalos) are identified using a variant version of Hierarchical Friends-of-Friends Algorithm (Klypin et al. 1999, HFOF), with the minimum particle number of 30. The close halo-halo pairs are selected in a way that they satisfy the observational criteria in both projected separation and in line-of-sight velocity difference to mimic the observed pairs. The halos in pairs can be either distinct halos (no smaller substructures contained or not hosted by a larger halo) or subhalos. For each halo, we compute its local density using the separation from its nearest n^{th} neighbor that is above certain mass cut M_{min}. Both n and M_{min} are determined so as to match the median distance to the 3^{rd}-nearest neighbor in the DEEP2 sample. Empirically, we found that $n = 6$ in the simulations traces the same comoving scale as $n = 3$ does in the observed data set. We note that the overall DEEP2 redshift completeness is $\sim 50\%$, which means that the observed 3^{rd}-nearest neighbor roughly corresponds to the 'true' 6^{th}- or 7^{th}-nearest neighbor. Therefore, our choice of $n = 6$ in the simulations should be a reasonable approach. In the rest of this paper, we refer δ_n to the overdensity measured using the 6^{th} nearest neighbor for halos. The resulting $(1+\delta_n)$ distribution of halos is very similar to the $(1+\delta_3)$ distribution of

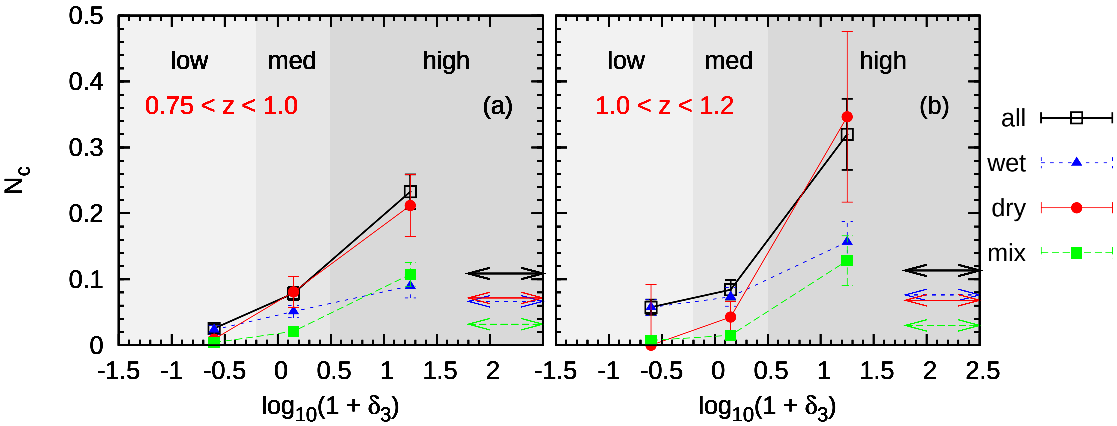

FIG. 3.— The pair fraction as a function of overdensity $(1+\delta_3)$. Here we show the results for four types of pairs: blue-blue pairs (blue triangles), red-red pairs (red solid circles), blue-red pairs (green solid squares), and all pairs regardless their colors (black open squares). The denominators used for computing the above four quantities are the numbers of blue, red, blue+red, and blue+red galaxies respectively. The error bars shown in the plot are calculated by bootstrapping. We set $N_c = 0$ and put the errors to be the Poisson errors for 5 objects when no pair is found at a given environment. The horizontal arrows appeared in the right-lower corner of each panel indicate the global pair fraction in the same redshift range taken from Lin et al. (2008) computed without separating data into different environment bins. There exists clear environment dependence of the pair fraction in the considered two redshift bins, being higher at denser environments.

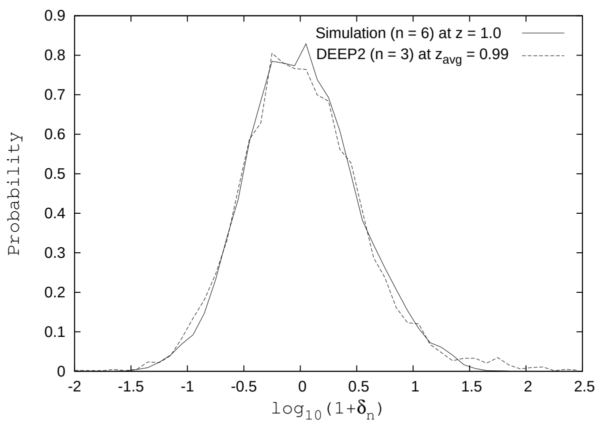

FIG. 4.— The overdensity $(1+\delta_n)$ distributions of the mock galaxy catalog (solid curve) and of the DEEP2 sample (dashed curve) at $z \sim 1$. The projected distance from the 3^{rd}-nearest neighbor is adopted to compute the overdensity for the DEEP2 sample; that of the 6^{th}-nearest neighbor is used for overdensity measurements in the mock galaxy catalog. The different choices of n^{th}-nearest neighbors between two samples are due to the spectroscopic incompleteness of the DEEP2 survey. Empirically we found that the adoption of $n = 6$ in the simulated galaxy catalog best reproduces the overdensity $(1+\delta_3)$ distribution function of the observed DEEP2 galaxies.

observed DEEP2 galaxies, as demonstrated in Fig. 4.

For each halo-halo pair identified with the criteria $r_p \leq 50$ h^{-1}kpc and $|\Delta v| \leq 500$ km s^{-1} , we trace their most-bounded 10 particles identified at a given epoch in the next adjacent few redshift frames. If 60% of these most-bounded 10 particles from the two pair components can be found in a single halo in the sequential frame, the pairs are then called to be merged. C_{mg} is thus computed as the fraction of pairs that will merge into a single halo. Among those merged halos, we record the time-scale T_{mg} over which the halo-halo pairs merge.

Fig. 5 displays C_{mg} and T_{mg} as a function of local density. It is interesting that while T_{mg} varies little with the local density, C_{mg} is a strong function of $(1+\delta_n)$, being smaller in higher density regions. This suggests that different environments have a strong impact on determining whether the close pairs will merge or not, but have little influence on the merger time-scale if those pairs are going to merge. When we analyze those halo-halo pairs that do not merge, we find that the majority of these pairs are actually widely separated in 3-D space and have large differences in 3-D velocity, and such projection effects are more pronounced for pairs in overdense environments. In the remainder of the cases, one component of the halo pairs may be tidally stripped and fails to be identified as a halo if they do not satisfy the virial condition in the next snapshot (Jian et al. 2008). In such cases, if the most-bounded particles do not belong to any halo, we then stop tracing their histories and count them as non-merging cases. We caution that this might underestimate C_{mg} in a way that the galaxy component may still survive temporarily until it merges with its companions, even though the dark matter of its hosting halos is stripped. However, if this is true, they will contribute to the tail of the T_{mg} distribution and hence shift T_{mg} toward a higher value. Because the merger rate is proportional to C_{mg} and inversely proportional to T_{mg}, such an effect will be roughly canceled out. To model the environment dependence of C_{mg}, we fit the curves in panel (a) of Fig. 5 by two lines:

$$C_{mg} = \begin{cases} (0.01z-0.08)x-(0.16z-0.85), & \text{if } x < 0 \\ (0.22z-0.45)x-(0.16z-0.85), & \text{if } x \geq 0, \end{cases} \quad (5)$$

where $x = \log_{10}(1+\delta_n)$.

In the simulations, the value of T_{mg} for pairs with $r_p < 50$ h^{-1}kpc is approximately 1 Gyr at $z \sim 1$, which is almost twice the typical value of ~ 0.5 Gyr adopted in previous studies (Lin et al. 2004, 2008) that used a more stringent criterium $r_p < 30$ h^{-1}kpc . The longer time-scale for such wider pairs has also been suggested in earlier works by Lotz et al. (2008b) who studied the merger time-scale using N-body/hydrodynamical simulations. We notice that T_{mg} increases slightly when going to lower redshifts. Because the simulations were stored at discrete epochs, the value of T_{mg} can only be estimated by

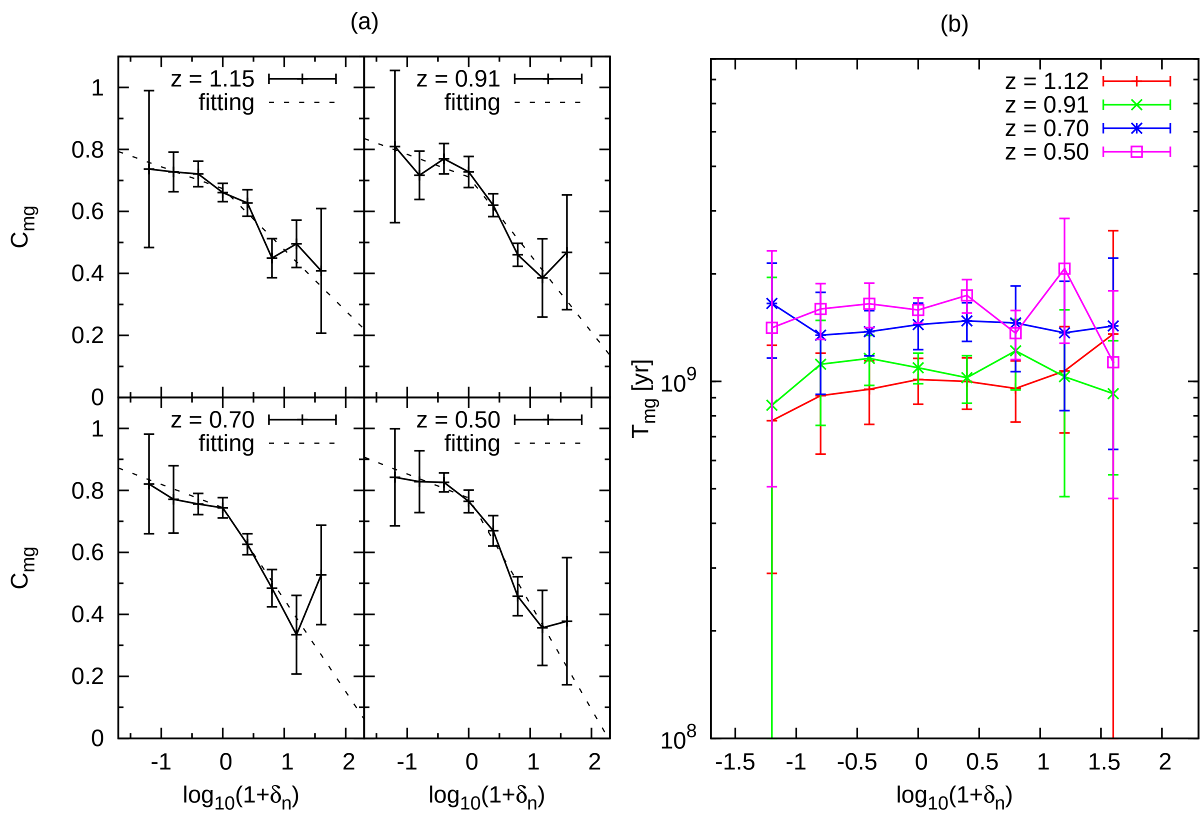

FIG. 5.— (a) C_{mg} (fraction of kinematic pairs to be merged) as a function of overdensity $(1+\delta_n)$, determined using the mock galaxy catalog constructed from the N-body simulations. The dashed lines represent the best-fitting formula of the data points. Over the entire redshift range we have probed, C_{mg} is a strong function of local environment. This is largely due to the stronger projection effects in overdense regions than that in underdense regions. The fitting formula of C_{mg} is given in Eq. 5. (b) T_{mg} (the merging time-scale) as a function of overdensity $(1+\delta_n)$ for those pairs that will eventually merge. The error bars represent the root-mean-squared of the scatter in each bin.

summing the time interval of several adjacent frames until the last frame in which the halos are identified as merged. In this way, T_{mg} is likely to be overestimated. However, since the time interval is typically $\sim$ 200 Myr at $z \sim 1$, which is much smaller than the typical time-scales normally found for pairs with $r_p < 50\ h^{-1}$kpc (Lotz et al. 2008b), we believe such uncertainty is negligible. Such an effect, on the other hand, becomes more apparent at lower redshift as the time interval between two adjacent redshift frames of the simulations rises to 400 Myr at $z \sim 0.4$. This might explain the trend of increasing T_{mg} with redshift. In this work, we adopt T_{mg} = 1 Gyr in all environment and C_{mg} derived with Eq. 5 when converting the pair fraction into the fractional merger rate as presented in the next section.

Before proceeding to compute the merger rate inferred from the pair fraction, it is worth discussing how our derived T_{mg} and C_{mg} are compared to previous works by other groups, in order to assess possible systematic errors in our estimates in the fractional merger rate. As we will see in §3.4, the fractional merger rate is proportional to C_{mg}/T_{mg}, here we use the ratio C_{mg}/T_{mg} as a comparison quantity. In our case, the typical value of C_{mg} is approximately 0.7 and T_{mg} is $\sim$ 1 Gyr averaged in all kind of environments, leading to C_{mg}/T_{mg} = 0.7. A recent study by Kitzbichler & White (2008) use the Millennium Simulation (Springel et al. 2005) to determine the averaged merger time-scale T_{mg} as a function of stellar mass and redshift of close pairs selected with various selection criteria (see Eq. (10) and (11) in Kitzbichler & White 2008). In their analysis, every pair will eventually merger; in other words, the effect of C_{mg} is absorbed into the quantity of T_{mg} (i.e., equivalent to set C_{mg} = 1). If adopting their Eq. (10) with h = 0.7, $r_p < 50\ h^{-1}$kpc and the stellar mass $M_* \sim 3 \times 10^{10} M_\odot$, which is the typical stellar masses in our pair sample, we get $T_{mg} \sim$ 2.7 Gyr. The ratio of C_{mg}/T_{mg} is thus 0.37, which is about half of our value of 0.7. This leads to a potential uncertainty by as large as a factor of two in the estimates of the fractional merger rate, depending on the adopted modeling of C_{mg} and T_{mg}.

3.4. *The Fractional Merger Rate f_{mg} as a Function of Environment*

In this section, we present our results on the fractional merger rate, defined as the fraction of galaxies in the range of $-21 < M_B^e < -19$ that merge per Gyr with another galaxy such that the luminosity ratio of the pair is between 4:1 and 1:4. This quantity can be derived from the pair fraction computed in §3.2 with the knowledge of C_{mg} and T_{mg} we have obtained in §3.3, but keeping in mind that the pair fraction in §3.2 is computed using pairs drawn from within a luminosity range of two magnitudes. Some true companions may fall outside the absolute magnitude range of our sample, while some selected companions have luminosity ratios outside the range of 4:1 to 1:4. To account for both of these effects, we use the following equation to convert the pair fraction into the fractional

merger rate f_{mg}:

$$f_{mg} = (1+G) \times C_{mg} N_c(z) T_{mg}^{-1}, \quad (6)$$

where G is the correction factor that accounts for the selection effect of companions due to the restricted luminosity range (see Lin et al. 2008 for the detailed computation of G). It is worth noting that the factor $(1+G)$ in Eq. 6 is different from $(0.5+G)$ that is shown in the Eq. (5) of Lin et al. (2008) due to different definitions between the merger rate (Lin et al. 2008) and the fractional merger rate adopted in this work.

In Fig. 6, we show the fraction merger rate, f_{mg}, as a function of overdensity for wet (blue points), dry (red points), mixed (green points), and all (black points) mergers. Those values are also listed in Table 1. Owing to the decreasing C_{mg} with overdensity, the increase of f_{mg} with respect to the overdensity is not as steep as N_c . However, we still find that the fractional merger rate in the overdense regions is, on average, 3-4 times greater than that in the underdense regions for all mergers regardless of their types, shown as black symbols in Fig. 6 (also see Table 1). Such enhancement in dense environments is in broad agreement with recent theoretical work by Fakhouri & Ma (2009) who measured the merger rates of friends-of-friends (FOF) identified mock matter halos in the Millennium simulation (Springel et al. 2005) as a function of local mass density. When dividing the merger sample into subcategories (wet, dry, and mixed mergers) we find a significant enhancement of the frequency of dry and mixed mergers between under- and overdense environments. In contrast, there is only a weak environment dependence between density extremes for wet mergers (Fig. 6). This implies that the group-like and cluster-like environment are preferred environments for dry and mixed mergers to take place.

At $z \sim 1$, the fractional dry merger rate in high-density regions is found to be 16±4% (Table 1), which is about 3 times larger than the global fractional dry merger rate derived from earlier studies (Lin et al. 2008; Bundy et al. 2009) regardless of their environments. An enhancement of dry mergers in overdense environments is also observed in the local universe. Using data drawn from the Sloan Digital Sky Survey (SDSS), McIntosh et al. (2008) find that the frequency of mergers between luminous red galaxies (LRGs) is higher in groups and clusters compared to that of overall population of LRGs by a factor of $2-9$ at $z < 0.12$. Our work similarly suggests that a greater probability for dry mergers in high density environments was already in place by at least $z \sim 1$. If we assume an average stellar mass ratio of 1:2 in our dry merger sample, a constant fractional dry merger rate in dense environments at $0 < z < 1$, and that all stellar mass involved in each merger is deposited into the final merger remnant, then we estimate that on average every local massive red-sequence galaxy in a dense environment is assembled through $0.16 \pm 0.04 (merger/Gyr) \times 7.7 (Gyrs) \sim 1.2 \pm 0.3$ major dry mergers, leading to $\sim (38{\pm}10)\%$ ($= 1.2 \times 0.5/(1+1.2 \times 0.5)$) mass accretion since $z \sim 1$.

4. DISCUSSION

4.1. *Comparison of the Environment Dependence of Merger Rates Between Observations and Simulations*

In this subsection, we discuss how our results are compared to previous theoretical predictions on the environment dependence of the merger rate of dark matter halos. There have been several attempts to investigate the relation between halo merger rates and underlying environments either using N-body simulations (Fakhouri & Ma 2009; Hester & Tasitsiomi 2009) or based on the Monte-Carlo merger trees that are constructed with the extended Press-Schechter (EPS) and excursion set models (Kauffmann & Haehnelt 2000). Using the Millennium simulation (Springel et al. 2005), Fakhouri & Ma (2009) measured the merger rate of dark matter halos as a function of the local mass density within a sphere of several Mpc using a friends-of-friends (FOF) algorithm. They found a strong dependence of specific halo merger rates on the environment, being greater in the densest regions than in voids by a factor of ~ 2.5. The level of enhancement of the specific halo merger rates in dense regions is in broad agreement with what we measure for observed galaxies. Very recent work by Hester & Tasitsiomi (2009) has also explored similar issues but for subhalos extracted from the Millennium simulations. In contrast, they find that in group environments, the subhalos are often tidally stripped and hence the chance of subhalo-subhalo mergers is low. As a consequence, the specific halo merger rate in groups is normally suppressed, which seems to be in contradiction to our finding that the fractional merger rate is enhanced in overdense environments.

However, we caution that direct comparisons between our results and simulations could be limited by several factors. For example, the studies by Fakhouri & Ma (2009) utilize the merger trees constructed from distinct FOF halos which do not correspond as well to observed galaxies as do the subhalos (substructures). Therefore translating their simulation results of halo merger rates into the actual merger rate of galaxies is not straightforward. On the other hand, the halo environment adopted in Hester & Tasitsiomi (2009) is based on the size/mass of the groups, characterized by the maximum of their rotation velocity curve, V_{max}. As shown in Fig. 2, there is spread in $(1+\delta_3)$ for a given number of group members, and vice versa, despite that in general the local density increases with the global environment (velocity dispersion, the number of group members, etc.). This suggests that at a given high local density in our sample, there are contributions from both the 'dense' field-like environments, as well as group-like and possibly even cluster-like environments. Therefore more adequate comparisons shall await larger surveys which sample mergers in various scales of galaxy groups and clusters.

4.2. *Are K+A Galaxies Formed Through Major Mergers?*

There have been several mechanisms proposed to quench the star formation in galaxies and lead to the formation of K+A galaxies. These mechanisms include galaxy-galaxy mergers (Mihos & Hernquist 1994), ram-pressure stripping (Gunn & Gott 1972), high speed galaxy encounters (galaxy harassment; Moore et al. 1996), and 'strangulations' in which the warm and hot gas is removed (Larson et al. 1980; Balogh et al. 2000). Except for galaxy mergers, many of those are strongly associated with the cluster environment. Several environment studies of poststarbursts have found a higher fraction of K+A galaxies in clusters than in the field (e.g. Tran et al. 2003, 2004; Poggianti et al. 1999). In contrast, other studies using large low-redshift samples have suggested that poststarbursts are preferentially found in the low density region (Balogh et al. 2005; Goto 2005; Hogg et al. 2006). Recently, Yan et al. (2009) studied the environment distribution of 74 K+A galaxies found at $z \sim 0.8$ in the DEEP2 redshift survey. They found that at this redshift range, there is very little environment dependence of the K+A fraction. Putting all these results together, it is suggested that the galaxy merger, which is not a cluster-specific mechanism, is potentially an

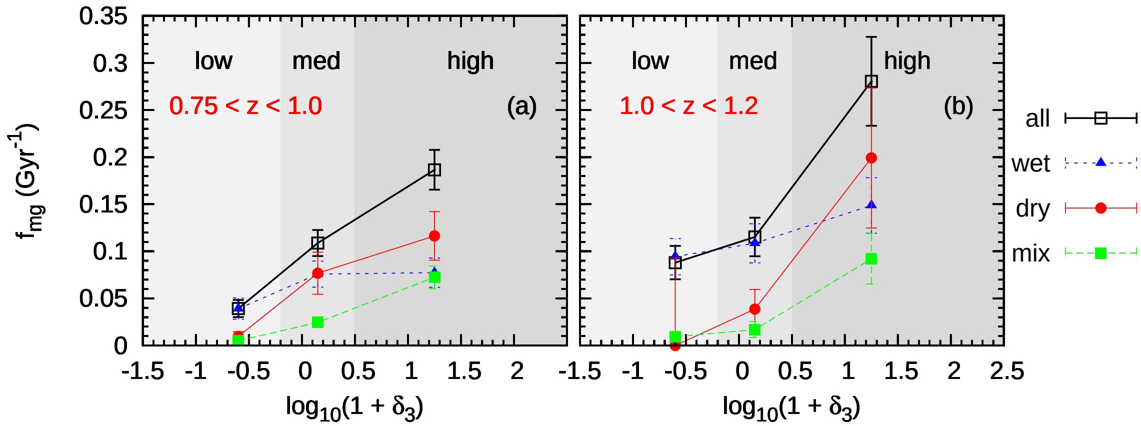

FIG. 6.— The fractional merger rate, f_{mg}, as a function of overdensity $(1+\delta_3)$. Here we show the results for four types of mergers: wet mergers (blue triangles), dry mergers (red solid circles), mixed mergers (green solid squares), and all pairs regardless of their colors (black open squares). The above four quantities have been normalized to the numbers of blue, red, blue+red, and blue+red galaxies respectively. The error bars are calculated by bootstrapping. We set f_{mg} = 0 and put the errors to be the Poisson errors for 5 objects when no pair is found at a given environment. While the fractional wet merger rate shows weak dependence on local density, the fractional rate of dry and mixed mergers strongly depends on the overdensity in the redshift range probed.

TABLE 1. THE FRACTIONAL MERGER RATE (f_{mg}) AS A FUNCTION OF DIFFERENT ENVIRONMENT

Merger Types	$\bar{z}$	N_c^a	N_c^b	N_c^c	G	C_{mg}^a	C_{mg}^b	C_{mg}^c	T_{mg}^a (Gyr)	f_{mg}^a (Gyr^{-1})	f_{mg}^b (Gyr^{-1})	f_{mg}^c (Gyr^{-1})
All	0.88	0.025±0.006	0.079±0.010	0.233±0.026	1.04	0.76	0.68	0.39	1.0	0.039±0.009	0.109±0.014	0.187±0.021
	1.08	0.058±0.012	0.084±0.015	0.032±0.054	1.10	0.73	0.65	0.42	1.0	0.088±0.018	0.115±0.020	0.281±0.047
Wet	0.88	0.024±0.007	0.051±0.009	0.090±0.018	1.19	0.76	0.68	0.39	1.0	0.039±0.011	0.076±0.014	0.077±0.016
	1.08	0.057±0.012	0.073±0.014	0.157±0.031	1.27	0.73	0.65	0.42	1.0	0.094±0.019	0.109±0.021	0.149±0.030
Dry	0.88	0.009±0.005	0.081±0.024	0.212±0.047	0.40	0.76	0.68	0.39	1.0	0.010±0.005	0.077±0.022	0.116±0.026
	1.08	0.000±0.092	0.043±0.023	0.347±0.129	0.38	0.73	0.65	0.42	1.0	0.000±0.093	0.039±0.021	0.199±0.074
Mixed	0.88	0.004±0.002	0.021±0.005	0.108±0.018	0.71	0.76	0.68	0.39	1.0	0.005±0.003	0.025±0.005	0.072±0.012
	1.08	0.007±0.004	0.015±0.008	0.128±0.038	0.72	0.73	0.65	0.42	1.0	0.009±0.005	0.017±0.008	0.092±0.027

[a] *low* density ($-1.0 < \log_{10}(1+\delta_3) < -0.2$)
[b] *median* density ($-0.2 < \log_{10}(1+\delta_3) < 0.5$)
[c] *high* density ($0.5 < \log_{10}(1+\delta_3) < 2.0$)

important origin of K+A galaxies found in the field. One way to test this hypothesis is to compare the environment distributions of K+A samples to that of the merger samples.

As shown in Fig. 6, the fractional wet merger rate in the DEEP2 sample depends weakly on the local density, similarly to the trend seen in DEEP2 K+A galaxies (see Fig. 6 of Yan et al. 2009). On the other hand, the mixed mergers show stronger dependence on the environment, unlike the K+A galaxies. In order to make more careful comparisons, we limit the K+A sample selected by Yan et al. (2009) with an additional restframe magnitude cut $-21.77 < M_B^e < -19.77$, which is 2 $\times$ brighter than the pair sample, to reflect the assumption that the K+A galaxies are products of two merging galaxies. We also apply the redshfit cut of $0.75 < z < 0.88$ to our pair samples so they span the same redshift range as the K+A galaxies. In Fig. 7, we plot the $(1+\delta_3)$ distribution of K+A galaxies against wet, dry, mixed, and wet+mixed pairs. Among the four types of pair samples, the density distributions of dry pairs and mixed pairs are distinct from that of the K+A sample, whereas wet pairs or wet+mixed pairs show similar a density distribution to the K+A galaxies. To quantify the significance of the environment difference or similarity between K+A samples and mergers, we perform three non-parametric statistical tests, the Kolmogorov-Smirnov test (K-S test), the Anderson-Darling test (A-D test; Anderson & Darling 1954; Pettitt 1976; Sinclair & Spurr 1988), and the Mann-Whitney-Wilcoxon test (MWW test; Mann & Whitney 1947) as done in Yan et al. (2009). The results are presented in Table 2. We find that the p-values derived from the K-S, A-D, and MWW tests for the K+A sample against dry and mixed mergers alone are all very close to the rejection threshold 0.05. On the other hand, the p-values for the wet vs. K+A set and the wet+mixed vs. K+A set are well beyond the threshold 0.05. Based on these results, we conclude that the environment distributions of K+A galaxies and of wet or wet+mixed mergers are indistinguishable. Nevertheless, we caution that such analysis is possibly limited by the small numbers of K+A and pair samples.

The idea that K+A galaxies could be formed through gas-rich mergers has also been tested using simulations by Bekki et al. (2005), who showed that the properties of K+A galaxies could be reproduced by merging two gas-rich systems, although the details depend strongly upon the orbital configuration. In addition, based on the kinematic study of K+A with integral field unit (IFU) spectroscopy for 10 nearby K+A galaxies, Pracy et al. (2009) found that the majority of their

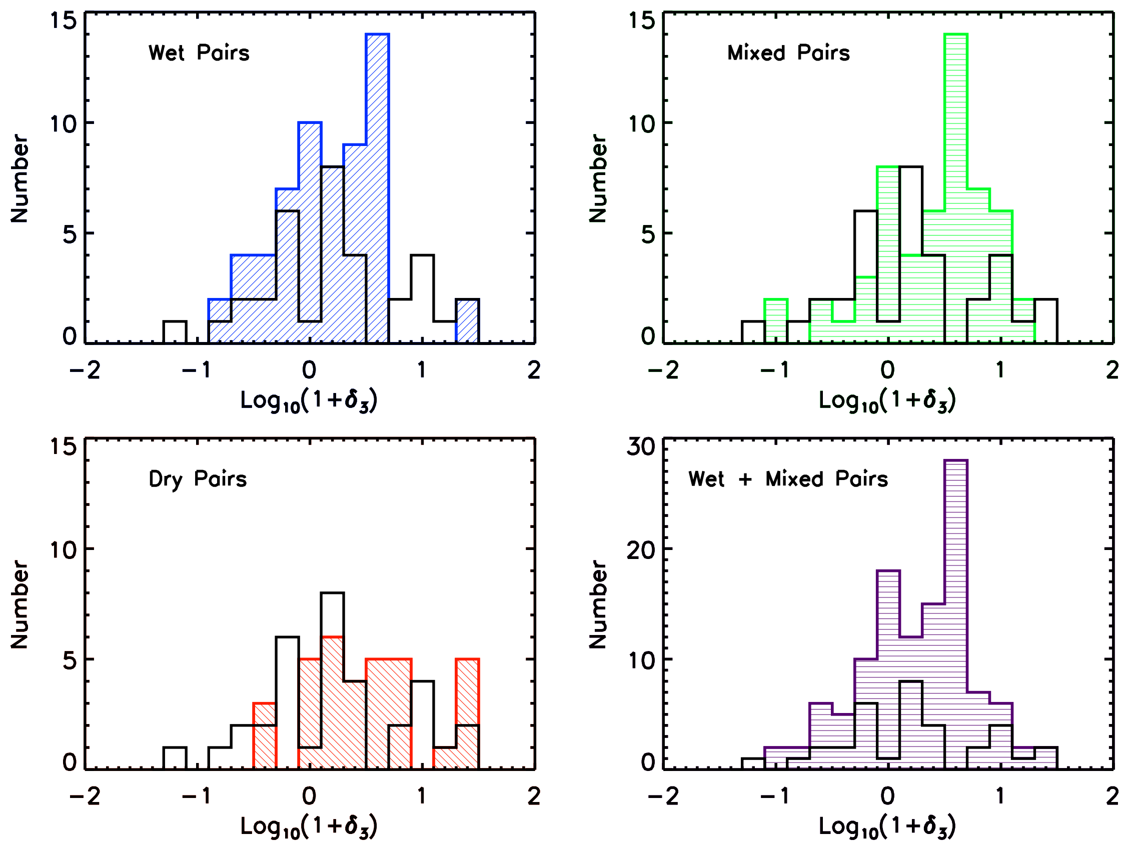

FIG. 7.— Comparisons of the overdensity $(1+\delta_3)$ distribution of K+A galaxies with candidates of wet (upper left panel), dry (lower-left panel), mixed (upper-right panel), and wet+mixed mergers (lower-right) respectively. The distributions of K+A galaxies are presented as black solid histograms while those of merger candidates are shown as color shaded areas.

K+A galaxies can be classified as 'fast rotators', which is consistent with a product of gas-rich mergers. However, whether our high-redshift K+A galaxies are subjected to the same mechanism that governs the low-redshift K+A formation is not well-understood (Yan et al. 2009). Although limited by small number statistics, our results at $z \sim 1$ are consistent with the scenario where wet mergers could be associated with the formation of K+A galaxies, and that mixed mergers might also contribute to some fraction of K+As, as mixed mergers together with wet mergers share similar environment distributions as K+As. Whether mixed mergers are able to quench the star formation of the gas-rich component and results in K+A phases will be an interesting topic to investigate further in simulations.

4.3. *The Role of Major Mergers in Forming Red-Sequence Galaxies*

It has been known that galaxy properties such as their colors, morphologies, and star formation histories depend upon the environment where they reside (Dressler 1980; Blanton et al. 2006; Cooper et al. 2006, 2007; Tasca et al. 2009, also see Kauffmann et al. 2004 for their discussion on the influence of stellar mass in addition to the environment). For example, the fraction of red, old, and S0/E types of galaxies increase in higher density regions (Dressler 1980). One class of processes is the so-called 'internal process', in which scenario galaxies evolve passively without interactions with other galaxies or the surrounding material such as IGM (Inter-Galactic Medium) or ICM (Intra-Cluster Medium). In this model, the average age of galaxies is older in dense regions simply because they have formed earlier than those in underdense regions. Other types of mechanisms are driven by the 'external process', including galaxy mergers, ram-pressure stripping, galaxy harassment, and strangulations as discussed in §4.2. It has become clear that passive evolution alone can not fully account for the change in the properties of galaxies across various environments, in particular the morphological transformations. Therefore the question is no longer whether the galaxies are evolved through 'nature' (internal) or 'nurture' (external) processes, but rather to what level do the external processes contribute to the evolution of galaxies and which extrinsic process is the dominant factor.

How does this paper relate to this subject? The derived fractional merger rate we derive suggest that galaxy mergers play a non-negligible role, in particular in dense environments. The higher frequency of dry mergers occurring in dense environments relative to underdense regions will lead to the following consequences: the structure parameters and the stellar mass function of red-sequence galaxies in dense environments should be different from those in underdense regions. This is because dry mergers tend to produce boxy, slowly rotating

TABLE 2. THREE STATISTICAL TESTS OF DIFFERENCES BETWEEN SAMPLES.

Subsamples	Kolmogorov-Smirnov	Anderson-Darling	Mann-Whitney-Wilcoxon test
wet vs. K+A	0.169	0.354	0.398
dry vs. K+A	0.085	0.078	0.039
mixed vs. K+A	0.011	0.079	0.057
wet+mixed vs. K+A	0.172	0.290	0.243

NOTE. — For most statistical tests, the values given above are the p-value, which gives the probability of the null hypothesis that the two samples are drawn from the same population. Conventionally the threshold significance level of 0.05 is adopted to rule out the null hypothesis.

anisotropic systems (Khochfar & Burkert 2005; Naab et al. 2006), and also increase the stellar mass per galaxy. The picture sketched above is in agreement with recent studies of the stellar mass function showing that red galaxies in dense environments are typically more massive than their counterparts in underdense regions (Bundy et al. 2006; Yang et al. 2009; Bolzonella et al. 2009).

Living at the high-mass extreme of the galaxy population in overdense environments are Brightest Cluster Galaxies (BCGs). In spite of the numerous studies of the properties of BCGs, their origin and evolution remain an unresolved issue. While there is evidence of on-going dry mergers found at the centers of groups and clusters at low and intermediate redshifts (Mulchaey et al. 2006; Rines et al. 2007; McIntosh et al. 2008; Tran et al. 2008; Liu et al. 2009), analyses based on stellar populations of BCGs indicate that BCGs have assembled most of the stellar mass ($\sim$ 90%) by at least $z \sim 1$, leaving little room for hierarchical assembling through mergers (Whiley et al. 2008; Collins et al. 2009). Whether the 38$\pm$10% mass accretion rate through dry mergers we derive in high-density regions is compatible with the $\sim$ 10% growth in the typical stellar mass of BCGs between $z = 1$ and $z = 0$ depends on the actual abundances of BCGs over this redshift range. The number density of massive halos at $z \sim 1$ is much lower than that at $z \sim 0$ in ΛCDM models. If the number of BCGs correlates with the number of massive halos in a similar manner between low and high redshifts, it is expected that a significant fraction of the progenitors of present-day BCGs has not appeared in the form of BCGs at $z \sim 1$ yet. In other words, the simplest explanation to alleviate the aforementioned potential discrepancy is that $z \sim 1$ BCGs only represent some portion of the present-day BCG population and the rest formed via successive dry mergers over this period. We remark, however, that our dry merger samples are likely going to be sub-BCG systems as very massive clusters are rare given our survey volume. Surveys over larger areas are required to tackle this issue more robustly.

The picture uncovered by this work can be summarized as follows. At $z \sim 1$ wet mergers occur at a similar rate across different environments ($\sim$ 0.06$\pm$0.01 per Gyr at $0.75 < z < 1.0$ and $\sim$ 0.12$\pm$0.01 per Gyr at $1.0 < z < 1.2$), while the frequency of dry and mixed mergers increases with the local galaxy density. The latter is primarily because of the increasing population of red galaxies with respect to local densities. As a consequence, while red-sequence galaxies in low-density environments are mainly built up through wet mergers, the dry and mixed mergers only become important at intermediate to overdense environments. Such events contribute to the assembly of massive red galaxies and could signal the precursors of BCGs in clusters seen in the local Universe. However, we caution that measurements of local density may not always have a one-to-one correspondence with the physical global environment (i.e., field, groups, and clusters). More accurate mapping of the relation between merger rates and the growth of massive galaxies in galaxy groups and clusters will have to await larger samples of interacting galaxies in those environments at low and high redshift.

5. CONCLUSION

Our results can be summarized as follows:

1. At $0.75 < z < 1.2$, the typical environment hosting mixed and dry mergers is denser than that of wet mergers, suggesting that the roles of wet, dry, and mixed mergers in the galaxy evolution vary with environment. The difference in the local density distribution of various types of mergers is in broad agreement with predictions based on the observed color-density relation. However, we noticed an excess of dry and mixed pairs compared to the above expectation toward overdense regions at a $\sim$ 2-σ level, indicating that the red and blue galaxies are not uniformly populated and there exists clustering effect at very small scales in those overdense environments.

2. In the redshift range ($0.75 < z < 1.2$) we have probed, we find a strong dependence of observed galaxy companion rate (N_c) on environment, which holds for all types of pairs (blue-blue, red-red, blue-red pairs). Although N_c increases with over density, using N-body simulations, we found that the fraction of pairs that will actually merge decreases with the local density. This is predominant because of a more pronounced projection effect in dense environments compared to low-density regions.

3. After correcting the environment dependence of the fraction of merger in pairs (C_{mg}) and the merger time-scale (T_{mg}), we find a weak environment dependence of the fractional merger rate for wet mergers over the redshift range $0.75 < z < 1.2$. The probability of a blue galaxy to merge with another blue galaxy is about 0.06$\pm$0.01 per Gyr at $z \sim 0.85$ and 0.12$\pm$0.01 per Gyr at $z \sim 1.1$. On the other hand, the fractional dry and mixed merger rate increases rapidly with local density due to the increased population of red galaxies in denser environments. The fraction of dry merger per Gyr is estimated to be (16$\pm$4)% in overdense regions.

4. We find that the environment distribution of wet mergers alone or wet+mixed mergers is indistinguishable from that of the K+A galaxies, suggesting a plausible link between K+A galaxies and wet and/or wet+mixed mergers.

5. While wet mergers transform galaxies from the blue cloud into the red sequence at a similar fractional rate across different environments, dry mergers are most effective in

high-density regions. We estimate that dry mergers contribute to (38±10)% mass accretion of massive red-sequence galaxies in overdense environments, such as BCGs in massive groups and clusters since $z \sim 1$. Based on our results, we therefore expect that the properties including structures and masses of red-sequence galaxies should be different between those in underdense regions and in overdenser regions since dry mergers are only important in dense environments.

We thank the anonymous referee for helpful comments to improve this paper. L. Lin would like to thank E. Barton, D. McIntosh, and C. Conselice for their helpful discussions. The work is partially supported by the National Science Council of Taiwan under the grant NSC99-2112-M-001-003-MY3. T. Chiueh and H.-Y. Jian acknowledge the support of NSC grant NSC97-2628-M-002-008-MY3. DEEP2 has been supported by NSF grants AST-0808133 and AST-0806732. The DEEP2 Redshift Survey has been made possible through the dedicated efforts of the DEIMOS instrument team at UC Santa Cruz and support of the staff at Keck Observatory. This work is also based in part on observations obtained with MegaPrime/MegaCam, a joint project of CFHT and CEA/DAPNIA, at the Canada-France-Hawaii Telescope (CFHT) which is operated by the National Research Council (NRC) of Canada, the Institute National des Sciences de l'Univers of the Centre National de la Recherche Scientifique of France, and the University of Hawaii. Access to the CFHT was made possible by the Ministry of Education and the National Science Council of Taiwan as part of the Cosmology and Particle Astrophysics (CosPA) initiative. We close with thanks to the Hawaiian people for use of their sacred mountain.

REFERENCES

Anderson, T. W.,& Darling, D. A. 1954, J. Am. Statist. Assoc., 49, 765
Balogh, M. L., Navarro, J. F., & Morris, S. L. 2000, ApJ, 540, 113
Balogh, M. L., Miller, C., Nichol, R., Zabludoff, A., Goto, T. 2005, MNRAS, 360, 587
Barton, E. J., Arnold, J. A., Zentner, A. R., Bullock, J. S., & Wechsler, R. H. 2007, ApJ, 671, 1538
Bell, E. F. et al. 2004, ApJ, 608, 752
Bell, E. F. et al. 2006, ApJ, 640, 241
Bell, E. F., Zheng, X. Z., Papovich, C., Borch, A., Wolf, C., & Meisenheimer, K. 2007, ApJ, 663, 834
Bekki, K.,Couch, W. J., Shioya, Y., Vazdekis, A. 2005, MNRAS, 359, 949
Binney, J. & Tremaine, S. 1987, Galactic dynamics (Princeton, NJ, Princeton University Press, 1987, 747 p.)
Blanton, M. R., Eisenstein, D., Hogg, D. W., & Zehavi, I. 2006, ApJ, 645, 977
Bluck, A. F. L.,Conselice, C. J., Bouwens, R. J., Daddi, E., Dickinson, M., Papovich, C., Yan, H. 2009, MNRAS, 294, 51
Blumenthal, G. R., Faber, S. M., Primack, J. R., & Rees, M. J. 1984, Nature, 311, 517
Bolzonella, M. et al. 2009, A&Asubmitted, preprint (arXiv:0907.0013)
Bundy, K. et al. 2006, ApJ, 651, 120
Bundy, K., Fukugita, M., Ellis, R. S., Targett, T., Belli, S., & Kodama, T. 2009, ApJ, 697, 1369
Carlberg, R. G., et al. 2000, ApJ, 532, L1
Cassata, P., et al. 2007, ApJS, 172, 270
Coil, A. L., et al. 2004, ApJ, 617, 765
Coil, A. L., et al. 2006, ApJ, 638, 668
Collins, C. A. et al. 2009, Nature, 458, 603
Conselice, C. J., Bershady, M. A., Dickinson, M., & Papovich, C. 2003, AJ, 126, 1183
Conselice, C. J. 2006, ApJ, 638, 686
Cooper, M. C., Newman, J. A.; Madgwick, D. S.; Gerke, B. F.; Yan, R.; Davis, M. 2005, ApJ, 634, 833
Cooper, M. C. et al. 2006, MNRAS, 370, 198
Cooper, M. C. et al. 2007, MNRAS, 376, 1445
Cucciati, O. et al. 2006, A&A, 458, 39
Darg, D. W., et al. 2009, preprint (arXiv:0903.5057)
Davis, M., Efstathiou, G., Frenk, C. S., & White, S. D. M. 1985, ApJ, 292, 371
Davis, M. et al. 2003, SPIE, 4834, 161
Davis, M. et al. 2007, ApJ, 660, L1
de Ravel, L. et al. 2009, A&A, 498, 379
Dressler, A. 1980, ApJ, 236, 351
Dressler, A. & Gunn, J. E. 1983, ApJ, 270, 7
Ellison, Sara L., Patton, David R., Simard, Luc, & McConnachie, Alan W. 2008, AJ, 135, 1877
Faber, S. M., et al. 2003, SPIE, 4841, 1657
Faber, S. M., et al. 2007, ApJ, 665, 265
Fakhouri, O., & Ma, C.-P. 2009, 394, 1825
Gerke, B. F. et al. 2005, ApJ, 625, 6
Gerke, B. F. et al. 2007, MNRAS, 376, 1425
Goto, T., 2005, MNRAS, 357, 937
Gunn, J. E., & Gott, J. R. I. 1972, ApJ, 176, 1
Hester, J. A., & Tastisiomi, A. 2009, preprint (arXiv:0902.4489)
Hogg, D. et al. 2004, ApJ, 601, L29
Hogg D. W., Masjedi M., Berlind A. A., Blanton M. R., Quintero A. D., Brinkmann J., 2006, ApJ, 650, 763
Hopkins, P. F., Hernquist, L., Cox, T. J., Di Matteo, T., Robertson, B., & Springel, V. 2006, ApJS, 163, 1
Jian, H.-Y., Chien, C.-H., & Chiueh, T. 2008, preprint (arXiv:0809.0978)
Jiang, C. Y., Jing, Y. P., Faltenbacher, A., Lin, W. P., & Li, C. 2008, ApJ, 675, 1095
Kitzbichler, M. G., & White, S. D. M 2008, MNRAS, 391, 1489 the Neutral Hydrogen Window", eds. R. Minchin and E. Momjian, AIP Conference Proceedings, in press
Kauffmann, G. & Haehnelt, M. 2000, MNRAS, 311, 576
Kauffmann, G., White, S. D. M., Heckman, T. M., Ménard, B., Brinchmann, J., Charlot, S., Tremonti, C., & Brinkmann, J. 2004, MNRAS, 353, 713
Khochfar, S. & Burkert, A. 2005, MNRAS, 359, 1379
Kitzbichler, M. G., & White, S. D. M. 2008, MNRAS, 391, 1489
Klypin, A., GottlAober, S., & Kravsov, A. V. 1999, ApJ, 516, 530
Lambas, D. G., Tissera, P. B., Alonso, M. S., & Coldwell, G. 2003, MNRAS, 346, 1189
Larson, R. B., Tinsley, B. M., & Caldwell, C. N. 1980, ApJ, 237, 692
Lin, L. et al. 2004, ApJ, 617, L9
Lin, L. et al. 2007, ApJ, 660, L51
Lin, L. et al. 2008, ApJ, 681, 232
Liu, F. S., Mao, S., Deng, z. G., Xia, X. Y., & Wen, Z. L. 2009, MNRAS, 396, 2003
Lotz, J. M., et al. 2008a, ApJ, 672, 177
Lotz, J. M., Jonsson, P., Cox, T. J., & Primack, J. R. 2008b, MNRAS, 391, 1137
Mann, H. B., & Whitney, D. R. 1947, The Annals of Mathematical Statistics, 18, 50
Marinoni, C., Davis, M., Newman, J. A., & Coil, A. L., 2002, ApJ, 580, 122
McIntosh, Daniel H., Guo, Y., Hertzberg, J., Katz, N., Mo, H. J., van den Bosch, Frank C., & Yang, X. 2008, MNRAS, 388, 1537
Mihos, J. C., & Hernquist, L. 1994, ApJ, 431, L9
Moore, B., Katz, N., Lake, G., Dressler, A., & Oemler, A, Nature, 379, 613
Mulchaey, J. S. et al. 2006, ApJ, 646, 133
Naab, T., Khochfar, S., & Burkert, A. 2006, ApJ, 636, L81
Nikolic, B., Cullen, H., & Alexander, P. 2004, MNRAS, 355, 874
Patton, D. R., Carlberg, R. G., Marzke, R. O., Pritchet., C. J., da Costa, L. N., & Pellegrini, P. S. 2000, ApJ, 536, 153
Patton, D. R., et al. 2002, ApJ, 565, 208
Patton, D. R., & Atfield, J. E. 2008, ApJ, 685, 235
Pettitt, A. N. 1976, Biometrika, 63, 161
Poggianti, B. M., Smail, I, Dressler, A, Couch, W. J., Barger, A. J., Butcher, H, Ellis, R. S., & Oemler, A., Jr. 1999, ApJ, 518, 576
Poggianti, B. M. et al. 2008, preprint (arXiv:0811.0252)
Pracy, M. B., Kuntschner, H., Couch, W. J., Blake, C., Bekki, K., & Briggs, F. 2009, preprint (arXiv:0903.4719)
Rines, K., Finn, R., & Vikhlinin, A. 2007, ApJ, 665, L9
Scarlata, C., et al. 2007, ApJS, 172, 494
Sinclair, C. D., & Spurr, B. D. 1988, J. Am. Statist. Assoc., 83, 1190
Skelton, R. E., Bell, E. F., & Somerville, R. S. 2009, ApJ, 699, L9
Springel, V. et al. 2005, Nature, 435, 629

Stewart, K. R., Bullock, J. S.,Barton, E. J., & Wechsler, R. H. 2009, ApJ, 702, 1005
Tasca, L. A. M. et al. 2009, A&A, 503, 379
Tran, K-V, Franx, M., Kelson, D., & van Dokkum, P. 2003, ApJ, 599
Tran, K-V, Franx, M., Illingworth, G., van Dokkum, P., Kelson, D., &Mages, D. 2004, ApJ, 609
Tran, K-v. H., Moustakas, J., Gonzalez, A. H., Bai, L., Zaritsky, D., & Kautsch, S. J. 2008, ApJ, 683, L17
van Dokkum, P. G., 2005, AJ, 130, 2647
Weiner, B. J., et al. 2005, ApJ, 620, 595
Wetzel, A. R., Cohn, J. D., & White, M. 2009, MNRAS, 395, 1376
Whiley, I. M. et al. 2008, MNRAS, 387, 1253
Willmer, C. N. A., et al. 2006, ApJ, 647, 853
Woods, D. F., Geller, M. J., & Barton, E. J. 2006, AJ, 132, 197
Yan, R., et al. 2009, MNRAS, 398, 735
Yang, X., Mo, H. J., & van den Bosch, F. C. 2009, ApJ, 695, 900
Yee, H. K. C., Ellingson, E., & Carlberg, R. G. 1996, ApJS, 102, 269